Icarus 293 (2017) 157–171

Contents lists available at ScienceDirect

Icarus

journal homepage: www.elsevier.com/locate/icarus

The role of very fine particle sizes in the reflectance spectroscopy of plagioclase-bearing mixtures: New understanding for the interpretation of the finest sizes of the lunar regolith

Giovanna Serventi[a,*], Cristian Carli[b]

[a] Department of Chemistry, Life Sciences and Environmental Sustainability, University of Parma, Viale delle Scienze 157/A, Parma 43124, Italy
[b] IAPS-Inaf, Viale Fosso del Cavaliere Tor Vergata, Roma, 00133 Italy

ARTICLE INFO

Article history:
Received 16 November 2016
Revised 6 April 2017
Accepted 18 April 2017
Available online 21 April 2017

ABSTRACT

The lunar surface consists of a regolith layer that covers the underlying bedrocks, and is generally characterized by particulates <1 cm. Lunar soil is the fine fraction of the regolith, and is generally between 60 and 80 μm. Sizes <10 μm, accounting for ca. 5–20% of the soil, were recognized and petrologically classified.

The coarsest sizes of the regolith are chemically and mineralogically similar, while the finest fractions are more feldspathic, probably due to easier fracturing of plagioclase than mafic minerals.

Due to the more feldspathic nature of the very fine lunar soils, in this paper, we quantitatively investigate the influence of very fine (<10 μm) plagioclase on the absorption bands of mafic minerals using the Modified Gaussian Model. We considered two plagioclases with different iron content and two mafic end-members (1) 56% orthopyroxene and 44% clinopyroxene, and (2) 30% orthopyroxene and 70% olivine. We also compared our results with the deconvolution of the same mixtures at coarser sizes. Our results mainly show that:

(1) fine sizes act principally on reflectance and on spectral contrast (with the former increasing and the latter decreasing); (2) very fine plagioclase has a blue slope in the Near Infrared and very shallow 1250 nm band depth, close to zero; (3) consequently, the plagioclase band is always shallower than mafic bands; (4) in mixtures with olivine, the composite band center always shows the typical olivine value, differently from coarser mixtures; and (5) mafic materials have a blue slope in the Short Wavelength Infrared Region, a more V-shaped 1 μm pyroxene absorption and the 1 μm mafic band centers are shifted by ca. 40 nm vs. coarse sizes, reflecting a different weight within the crystal field absorption of the mafic component in very fine size. We also evidenced that a coarse plagioclase could be overestimated, while a very fine one could be underestimated if compared with the 63–125 μm size.

1. Introduction

Very fine sizes dominate many planetary surfaces and their regolith, e.g., Moon, Mars and Mercury. Different particle size fractions in the regolith (such as soil and dust) affect the optical properties of the surface in different ways. For this reason, very fine particles and their effects on the reflectance spectra of the most common planetary minerals have to be investigated in detail to obtain correct information about the mineralogical composition and the surface texture.

In particular, the lunar surface consists of a regolith layer that covers the underlying bedrocks, with the exception of steep-sided crater walls, central peaks and lava channels (McKay et al., 1991), as shown by the lunar landings and observations. Due to the absence of atmosphere on the Moon, the lunar regolith is the result of different processes, e.g., the impact of meteoroids and bombardments of protons from the sun and the stars, and is generally considered to be characterized by material lower than 1 cm in size (McKay et al., 1991). The fine fraction of the regolith, deriving from mechanical disintegration of lunar rocks, both basaltic and anorthositic, constitutes the lunar soil. The average lunar soil size is generally between 60 and 80 μm (McKay et al., 1991). Lunar dust consists of even finer material than lunar soils (ca. <50 μm). Furthermore, sizes <10 μm, which comprise ca. 5–20% of the soil,

* Corresponding author.
E-mail addresses: giovanna.serventi@unipr.it (G. Serventi), cristian.carli@iaps.inaf.it (C. Carli).

http://dx.doi.org/10.1016/j.icarus.2017.04.018
0019-1035/

have been recognized and petrologically classified (Laul et al., 1978, 1979, 1980).

Silicate minerals, such as orthopyroxene (OPX), clinopyroxene (CPX), olivine (OL) and plagioclase (PL), are the most important constituents of the lunar surface, associated with oxides (e.g., Papike et al., 1991), and can be spectrally identified on the basis of their absorption bands. While the iron-richer mafic minerals have always been easily detected (e.g., Tompkins and Pieters, 1999; Spudis et al., 1984), only recently, and thanks to the improvements in spectrometers onboard during the last missions, the absorption due to the low amount of Fe^{2+} in PL could be detected (e.g., Ohtake et al., 2009; Cheek et al., 2012a,b; Kramer et al., 2013), permitting new evaluation of its modal abundance and composition.

While coarse sizes of the regolith are chemically and mineralogically very similar, the finest fractions, <10 μm, are different and more feldspathic. This may be due to simple comminution processes and easier fracturing of PL than to mafic minerals (Laul et al., 1978, 1979, 1980; Devine et al., 1982).

According to the more feldspathic nature of the very fine lunar soils, in this paper we present results for a set of PL-bearing mixtures analyzed at the <10 μm particle size, also proposing a comparison with coarser mixtures analyzed by Serventi et al. (2013, 2015), to investigate the effects of very fine sizes on the reflectance spectroscopy of lunar-like minerals.

2. Background

2.1. PL and PL-bearing mixtures

Only in the last decade, PL and PL-bearing mixtures have been studied in detail, since the improvements in terms of spectral resolution of the spectrometers onboard in lunar missions permitted to clearly recognize the PL absorption band at ca. 1250 nm due to Fe^{2+} transition in its crystal structure (Adams and Goulland, 1978; Burns, 1993).

Cheek et al. (2011) demonstrated that in a set of synthetic An_{85} PL with different iron content, the 1250 nm band deepens as the iron content increases, up to a maximum value (ca. 0.4 wt.% FeO) after which the band depth remains quite constant.

Serventi et al. (2013, 2015) showed that PL can be easily recognized in mixtures with pyroxenes (PX) for modal abundance higher than 70%, while in mixtures with OL it can be masked due to the narrow spectral range, in which both OL and PL absorb, thus creating a complex, composite (COMP) absorption. Moreover, spectral parameters, Gaussian modeling and Hapke modeling show that PL can spectrally influence the absorption of mafic minerals (Serventi et al., 2013, 2015; Carli et al., 2014).

Cheek and Pieters (2014) analyzed PL-rich mixtures with varying content and composition of OL, PX and very high-Mg spinels and demonstrated that PL can significantly contribute to reflectance spectra if strongly absorbing minerals are present in low abundances, particularly in mixtures with PX.

Serventi et al. (2016) concluded that, in PL-dominated mixtures: (1) PL can be an important contributor to reflectance spectroscopy also affecting mafic mineral absorption bands (as also demonstrated by Cheek and Pieters, 2014); (2) PL absorbs in the 1250 nm spectral region but iron-rich PL also affects the longest wavelengths (1600–1800 nm), as also suggested by Pieters (1986) and Hiroi et al. (2012); and (3) PX are easily recognizable in mixtures with PL, even at very low PX concentration (~1%), while OL, if less than 5%, can be masked by iron-rich PL.

2.2. Particle size

Generally, variation in particle size affects albedo, reflectance and spectral contrast; in particular, as the particle size decreases albedo increases, while spectral contrast, meant as the strength of absorptions, is reduced due to the decrease in the mean optical path length of reflected light (Adams, 1968; Pieters, 1983). On the other hand, band centers and band widths are almost unaffected by different particle sizes (Nash and Conel, 1974), or show shifts that fall in the spectral resolution of the instruments (Serventi et al., 2013).

Crown and Pieters (1987) evaluated the reflectance spectra of mixtures composed of different modal abundance of labradorite (An_{80} PL) and enstatite (Mg-OPX) at different particle sizes. The authors showed that, in the spectra of both end-members and mixtures, by reducing the size reflectance increases and the spectral contrast decreases. In addition, they pointed out that the amount of PL detectable in mixtures with mafic minerals is particle size dependable: more PL is required in finer mixtures.

Mustard and Hays (1997) investigated the effects of fine particles that are approximately the same size as the wavelength of light on reflectance spectra of OL and quartz (in the 0.3–25 μm spectral range). In particular, spectra exhibit a drop in reflectance with the finest sizes. Looking at their Fig. 4, in the 300–2500 nm range, as the size becomes finer, OL albedo increases while the spectral contrast decreases. Furthermore, the slope in the NIR is less red as size decreases. On the contrary, looking at their Fig. 5, quartz's albedo does not change linearly with the particle size; however, the broad absorption at ca. 1000–3000 nm disappears at very fine sizes.

Furthermore, the transparency features show several important changes as particle size decreases: the spectral contrast increases then decreases, the position of the maximum reflectance of the transparency features shifts systematically to shorter wavelengths, and the symmetry of the features changes.

Cooper and Mustard (1999), analyzing Martian analog minerals (e.g., montmorillonite and palagonite), concluded that extremely fine particle sizes generate significant decreases in band strength. In particular, the <5 μm fractions showed vibrational absorption bands that were half the strength of the absorptions from the coarser size fractions. They also concluded that this reduction is due to changes in the ratio of scattering to absorption along with changes in particle size, with important implications for the spectroscopic determination of the composition of the extremely fine Martian dust.

Craig et al. (2007) evidenced that, as particle size increases, the overall reflectance of OL, OPX and basalts decreases, while the bands deepen to reach a maximum between 45 and 250 μm and then decrease. Particle size coarsening can also produce band saturation effects that complicate the determination of the absorption band center.

Serventi et al. (2013, 2015, 2016) showed that different particle sizes (125–250 μm; 63–125 μm; 36–63 μm) of PX, OL and PL spectra do not affect the band center (shifts of few nanometers fall within the instrumental resolution) but only the band depth, which decreases as the particle size decreases.

3. Experimental procedure: sample preparation and analytical methods

3.1. End-member preparation and characteristics

Separate end-member minerals were obtained from samples belonging to the Stillwater Complex layered intrusion. The samples were accurately investigated under thin section to evidence the rock mineral association and to reduce altered samples as much

Table 1
Mineral abundances in the starting samples. OPX = orthopyroxene; CPX = clinopyroxene; OL = olivine; PL = plagioclase; Op = opaque minerals; Zois = zoisite. Table also shows the applied amperage (Amp.), the minerals removed and the final samples obtained with the Frantz Isodynamic Magnetic Separator. Chemistry and iron abundance of the new samples are also reported.

Lithology	Mineral abundance						Amp.	Minerals removed	New samples	Chemistry	FeO wt.%
	OPX %	CPX %	OL %	PL %	Op %	FeO wt. %					
Ultramafic rock	47	–	19.7	5.1	28.3	FeO wt. %	0.3	Op	CPX+OPX+OL(E3)	OPX(28.2%) En_{82}-Wo_4	9.03
							1.4	PL			3.8
										CPX(3.4%) En_{45}-Wo_{46}	14.65
										OL(68.4%) Fo_{84}	
Anorthosite	0.8	4.3	–	94.2	–	FeO wt. %	1.4	CPX+OPX+Zois.	PL(PL3)	PL3 An_{80}	0.36
Gabbronorite	22.1	17.3	–	60.6	–	FeO wt. %	1.4	None	CPX+OPX(E1)	CPX(43.9%) En_{45}-Wo_{46}	5.72
									PL(PL2)		0.5
										PL2 An_{80}	13.45
										OPX(56.1%) En_{77}-Wo_2	

as possible (Carli et al., 2009). From among the different samples, we selected an anorthosite, a gabbronorite and an ultramafic rock (for the composition, please refer to Table 1). The chemistry of the rock-forming minerals was determined by electron microprobe analyses with a CAMECA SX50 (EMP) at the microprobe laboratory of C.N.R.-IGG (Consiglio Nazionale delle Ricerche, Geosciences and Earth Resources), Padua, Italy.

The selected rock samples were first crushed to a coarse size class <2.00 mm, in order to preserve the original rock composition in powdered samples. The powders were then quartered and each fraction was ground to smaller size classes. In particular, we have considered two particle-sizes, <250 µm and <125 µm. Each powder particle-size class was then quartered again and half of the material was then sieved into two size ranges: 63–125 µm and 125–250 µm. The size fractions were produced by dry sieving; we decided not to perform wet sieving to avoid: (1) possible alteration or contamination; (2) leaching, which can settle the size distribution of our samples, differently from what expected in atmosphereless planetary conditions.

From these samples, two PLs with different iron content and two different mafic, multimineralic compositions were separated using a Frantz Isodynamic Magnetic Separator at the Department of Chemistry, Life Sciences and Environmental Sustainability, University of Parma, Italy. Table 1 shows the applied amperage, removed minerals and new samples obtained after magnetic separation. The purity of the end-members was determined with optical means (X-ray diffraction was ruled out since it is not accurate for phase abundance less than 5%).

The selected PL phases include a medium-iron (PL2) and an iron-rich (PL3) PL (both An_{80}, with 0.36 and 0.5 wt. % FeO, respectively), while the Fe, Mg (mafic) compositions consist of two distinct mineral assemblages, one PX-bearing (E1), and one OL-rich and PX-poor (E3). The Fe, Mg phases were also analyzed with Mössbauer spectroscopy, in order to have a better comprehension of the iron oxidation state (for further details, please refer to Serventi et al., 2013). The fitting of Mössbauer results showed the absence of additional phases.

3.2. Mixture preparation

Mixtures of Fe, Mg (E1, E3) and PL (PL2, PL3) end-members were prepared at two different particle sizes (63–125 and 125–250 µm). For each particle size, contents ranging between 20 and 90 wt. % of each PL end-member were added to each Fe, Mg end-member.

For each of the resulting mixtures, we calculated the vol. FeO% due to PL phase with respect to the mixture. The volumetric FeO% was calculated as the FeO wt. % content in PL multiplied by modal PL (%) in each mixture. All the results presented in this work have been plotted vs. the vol. FeO in PL.

Starting from the 63–125 µm mixtures and end-members, very fine sizes (<10 µm) were produced using a micronizer at the Department of Geosciences, Padua, Italy. Each powder, with the addition of water to prevent the heating of the sample, was micronized for 5 min; the very fine powder plus water was mixed with ethanol and kept in stove for ca. 2 weeks, until all the water, and ethanol, evaporated. Then, the very fine powders were weighed to check that no material was lost during the mechanical grinding.

3.3. Spectral measurements

Bidirectional reflectance spectra of each mixture were acquired at room temperature and normal atmospheric pressure with a Field-Pro Spectrometer ® mounted on a goniometer (Istituto di Astrofisica e Planetologia Spaziali, Inaf-IAPS, Rome, Italy). The spectra were acquired with a spectral resolution of ~3 nm in the VIS and of ~10–12 nm in the NIR and spectral sampling of 1 nm, with $i = 30°$ and $e = 0°$ The source used was a QTH (Quartz Tungsten Halogen) lamp and the spot illuminated had an area of ca. 0.5cm^2. The calibration of the spectrometer was performed with Spectralon® optical standard (registered trademark of Labsphere, Inc.).

Ten spectra were acquired for each powder, emptying and refilling the cup each time, and then only the mean spectrum was considered for subsequent analyses. In order to avoid problems due to a pressed surface with a "slab-like behavior" or to coarser powder roughness due to the aggregation of such fine particles, powders were gently shaken and pressed in the sample holder.

Fig. 1 shows the end-member spectra; mixture spectra are plotted in Figs. 2 and 3, while the continuum-removed spectra of end-members and mixtures are reported in Fig. 4. As a comparison, reflectance spectra of coarser sizes (63–125 µm and 125–250 µm) are shown in Figs. 2 and 3.

3.4. MGM deconvolution

Each spectrum was analyzed applying the Modified Gaussian Model (MGM) algorithm (Sunshine et al., 1990). In short, we considered a fixed continuum tangent to the spectrum reflectance maxima as more reliable in the description of the spectrum shape and for modeling the strength of the absorption bands (approach already followed by Clenet et al., 2011 and Serventi et al., 2015).

First, we deconvolved the end-members, mafic and PL, as mineralogically unknown end-members, assigning Gaussians only where either an absorption band or a band asymmetry was visually perceptible (e.g., 900 nm band in E1 is asymmetric towards the Near Infrared – NIR - region). Then, we deconvolved the mixtures:

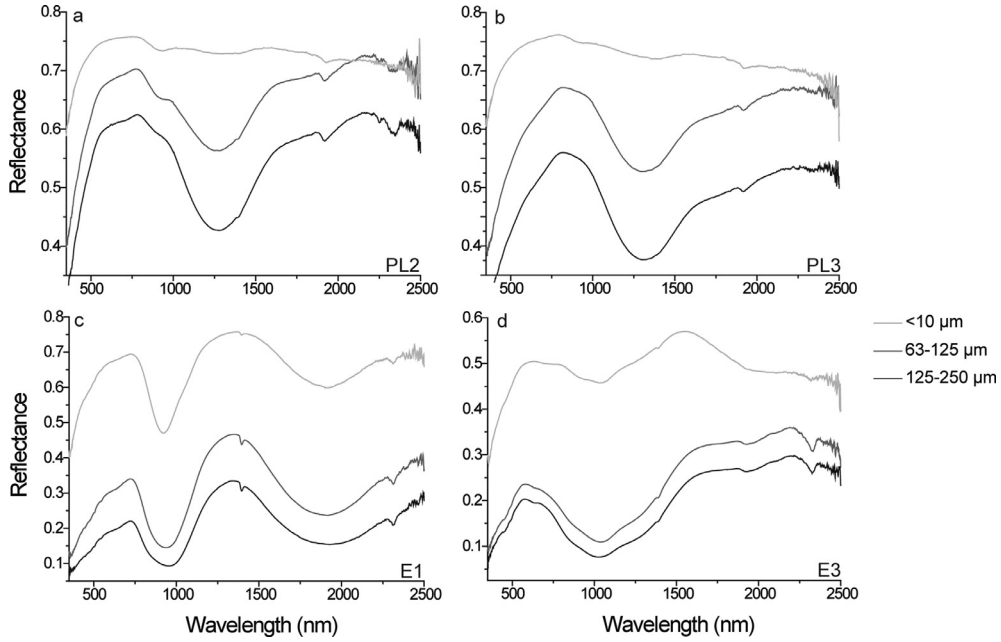

Fig. 1. End-member reflectance spectra at three different particles sizes, 125–250 µm (black), 63–125 µm (dark gray) and <10 µm (light gray). Generally, reducing the particle sizes the albedo increases and the spectral contrast is reduced. (a, b) Very fine PL are characterized by featureless spectra with a blue slope; (c) very fine E1 shows a 900 nm band shifted towards shorter wavelengths and more asymmetric towards the NIR with respect to the coarse sizes; and (d) the fine E3 complex 1050 nm band is characterized by three multiple absorptions, but the absorption centered at ca. 1250 nm seems shallower with respect to the coarse sizes and is evident the appearance of an absorption at 2000 nm. (For interpretation of the references to colour in this figure legend, the reader is referred to the web version of this article.)

Table 2
In the table are reported a list of Gaussians used in the end-member deconvolution, the wavelength position and the mineralogical interpretation.

Gaussian	Position (nm)	Interpretation
G1	900–950	Fe^{2+} in OPX M2 site
G2	1000–1100	Fe^{2+} in CPX M2 site
G3	1850–2000	Fe^{2+} in OPX M2 site/ chromite
G4	2200–2300	Fe^{2+} in CPX M2 site/ Al-OH alterations
G5	840	Adjustment Gaussian
G6	850–950	Fe^{2+} in OL M1 site
G7	1000–1100	Fe^{2+} in OL M2 site
G8	1200–1250	Fe^{2+} in OL M1 site
G9	1200–1300	COMP band (Fe^{2+} in OL M1 site+Fe^{2+} in PL)
G10	1250–1300	Fe^{2+} in PL
G11	1600–1800	PL asymmetry/PL alteration

1) fixing band center and band width assigned to the mafic end-member absorption bands, with the exception of 1800–2000 nm absorption band width that became visually narrower as PL increased;
2) leaving the mafic band depth free, which depends on mineral abundance in a mixture (e.g. Sunshine and Pieters, 1993; Serventi et al., 2015), and Gaussian parameters assigned to the 1250 nm absorption band (for further details, interested readers are referred to Serventi et al., 2015).

A visual check of the residuals after the fitting evidenced a pattern in the 700–1100 nm spectral range of the E1-bearing mixtures not detected at coarser sizes. For this reason, starting from values obtained from the fit with the procedure described above, we recomputed MGM leaving the mafic parameters free (see Section 4.3).

A number was assigned to each Gaussian, as described in Table 2.

4. Results

4.1. End-member and mixture reflectance spectroscopy

A comparison between the end-members is plotted in Fig. 1. In particular, considering the very fine size, (1) PL spectra (Fig. 1a,b) are characterized by a blue slope in the NIR and are almost featureless; (2) E1 900 nm band becomes V-shaped (Fig. 1c) and the band asymmetry towards the NIR is emphasized. This asymmetry seems to be correlated to a shift of the 900 nm band towards shorter wavelengths, as if OPX became even more dominant than CPX as the size decreased; (3) the E3 complex 1050 nm band (Fig. 1d) is characterized by three multiple absorptions due to the Fe^{2+} transitions in OL M1 and M2 sites, but the absorption centered at ca. 1250 nm seems shallower with respect to coarser sizes; (4) mafic assemblages (Fig. 1c,d) show a more marked blue slope in the short wavelength infrared region (SWIR) with respect to the coarsest size, and (5) E3 (Fig. 1d) shows the appearance of an evident absorption at 2000 nm.

Both E1 and E3 indicate more influencing OPX reflectance properties than other mafic phases such as OL, CPX. However, the rock sample from which E3 was magnetically separated contains 2% of chromite. Even if the residual chromite in our sample after separation is very low (<<0.5%), chromite is characterized by a deep absorption at ca. 2000 (e.g. Cloutis et al., 2004), and, thus, we cannot completely rule out chromite as a contributor to the 2000 nm absorption.

PL end-members were magnetically separated from rocks containing PX. The separated PL was investigated by optical microscope analysis with no detection of residual PX, but we have to consider that PX inclusions could still be present. For this reason, the 900 nm band showed by PL spectra in Fig. 1a could be indicative of residual PX. Furthermore, Fig. 1b reveals that a fine size emphasizes the effects of residual PX; the 900 nm band due to Fe^{2+} in PX becomes more absorbing as size decreases (see also the continuum-removed spectrum in Fig. 4b).

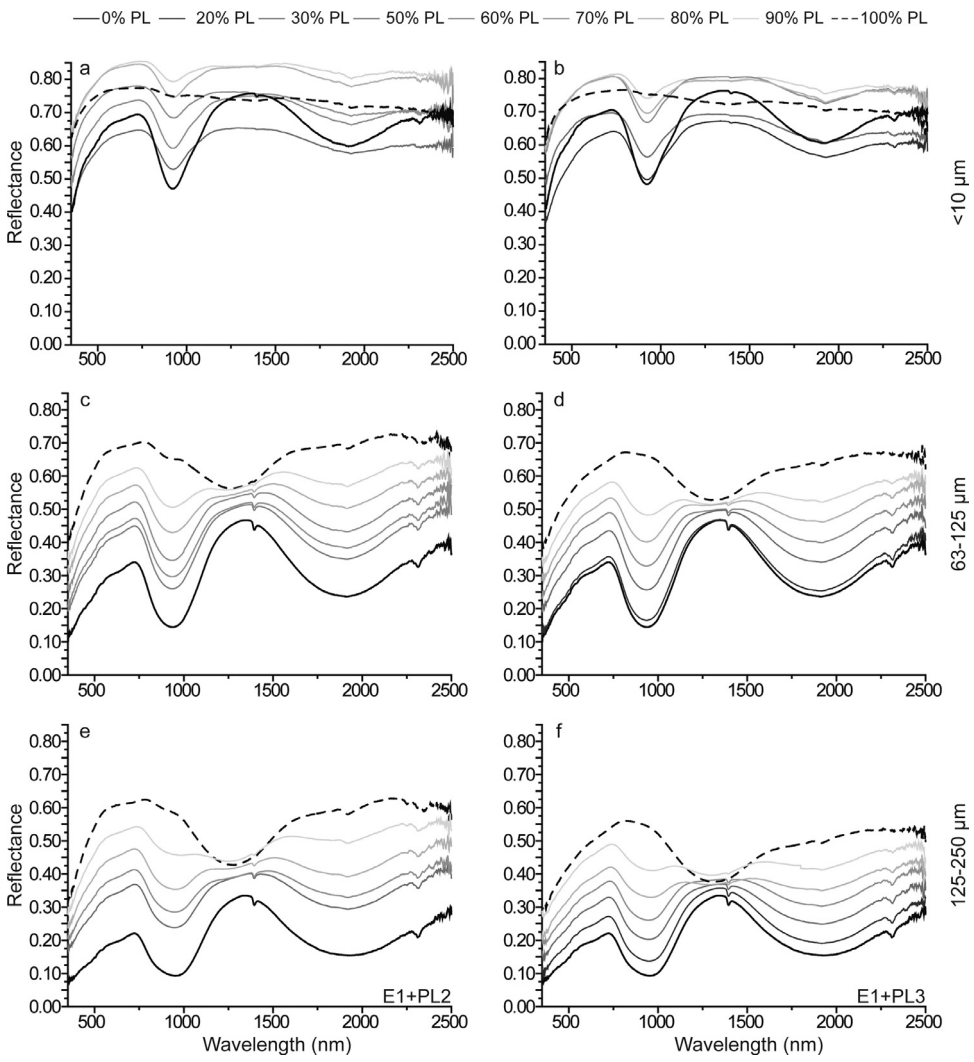

Fig. 2. Reflectance spectra of E1-PL mixtures at three different particle sizes. (a, b) E1+PL2 and E1+PL3, <10 µm; (c, d) E1+PL2 and E1+PL3, 63–125 µm; and (e, f) E1+PL2 and E1+PL3, 125–250 µm. Generally, a fine particle size produces spectra with higher reflectance and reduced spectral contrast compared to the coarsest sizes.

Figs. 2 and 3 show that a fine particle size (Fig. 2a,b and 3a,b) increases reflectance and reduces spectral contrast compared with the coarsest sizes (Fig. 2c–f and 3c–f).

Considering the 63–125 and 125–250 µm sizes (Figs. 2c–f and 3c–f), a higher PL modal abundance entails a systematic increase in reflectance, whereas, in the <10 µm size, some spectra deviate from this behavior, such as the 70%PL3-E3 and the PL end-members (see Figs. 2a,b and 3a,b). As explained in Section 3, working with such fine sizes means dealing with problems caused by too pressed surfaces or to powder roughness. For this reason, spectra acquired on the same sample have variable reflectance values, with the mean spectrum showing a standard deviation up to ca. 6%, which can explain the reflectance behavior that is not linear with the increase in PL modal abundance.

PL in very fine E1-bearing mixtures results in a weaker absorption band than for coarse sizes and is revealed by a flattening in the 1200 nm spectral region for 80% PL-mixture (Fig. 4a,b). A weak absorption band can be recognized only for more than 90% PL (light-grey spectra in Fig. 4a,b), but always shallower than PX absorption bands.

Serventi et al. (2013) demonstrated that the spectral parameters describing the COMP band, due to the simultaneous absorptions of OL and PL, give information on the relative minerals' modal abundance. In particular, considering coarse E3-bearing mixtures, the COMP band center shifts from typical OL values (1050 nm) to PL values (1250 nm) for PL content >70% (see their Fig. 13b). However, investigating the <10 µm size, the center shifting is not detectable (Fig. 4c,d); this is consistent with the featureless nature of PL.

4.2. End-member deconvolution

End-members were deconvolved via MGM (see Fig. 5a and 6a; to show the goodness of the fit, RMS is plotted). E1 residual (Fig. 5a, h) shows a sinusoidal pattern in the 700–1100 nm; comparing our residuals to those by Klima et al. (2008), which showed the same pattern and the same RMS as ours, we decided not to add additional Gaussians.

A comparison with the deconvolution of coarser sizes (see Table 3) demonstrates that the 900–1000 nm absorptions are fitted with the same number of Gaussians, with the only exception of E1, where an adjustment Gaussian (G5) centered at ca. 840 nm has not been used (in accordance with Klima et al., 2007). Despite the end-member residual seems to indicate a sinusoidal pattern, the covariance matrix does not allow more Gaussians to be added. Moreover, a similar residual pattern is present also in Klima et al. (2007, 2011). On the contrary, G5 is required for coarser size as discussed in Serventi et al. (2015, 2016) and in accordance with Sunshine and Pieters (1993).

Table 3
In table are reported the spectral parameters obtained by MGM deconvolution of mafic end-members, at the 63–125 μm (on the left), 125–250 μm (on the central column) and <10 μm (on the right). Center and width are expressed in nanometers, while depth as the logarithm of the reflectance. RMS represents the Root Mean Square error: the lower the RMS the better the fit. To show the goodness of the fit, for band center, the error calculated at 95% level of confidence was reported.

E1												
	63–125 μm				125–250 μm				<10 μm			
	Center	Width	Depth	RMS	Center	Width	Depth	RMS	Center	Width	Depth	RMS
G5	843 ± 9	110	−0.400		837 ± 6	113	−0.370					
G1	934 ± 9	159	−0.929		949 ± 30	180	−0.895		903 ± 10	154	−0.252	
G2	1028 ± 20	199	−0.535		1058 ± 30	191	−0.371		988 ± 10	220	−0.217	
G3	1851 ± 11	496	−0.766		1813 ± 15	489	−0.631		1894 ± 10	509	−0.194	
G4	2311 ± 50	730	−0.431		2202 ± 50	678	−0.586		2321 ± 40	138	−0.025	
				0.018				0.020				0.06
E3												
	63–125 μm				125–250 μm				< 10 μm			
	Center	Width	Depth	RMS	Center	Width	Depth	RMS	Center	Width	Depth	RMS
G6	861 ± 7	210	−0.464		842 ± 2	193	−0.483		881 ± 10	163	−0.063	
G7	1028 ± 6	204	−0.562		1009 ± 2	218	−0.722		1036 ± 8	241	−0.139	
G8	1221 ± 3	400	−0.655		1221 ± 2	408	−0.789		1262 ± 10	296	−0.08	
G3									1963 ± 2	442	−0.080	
				0.005				0.003				0.005

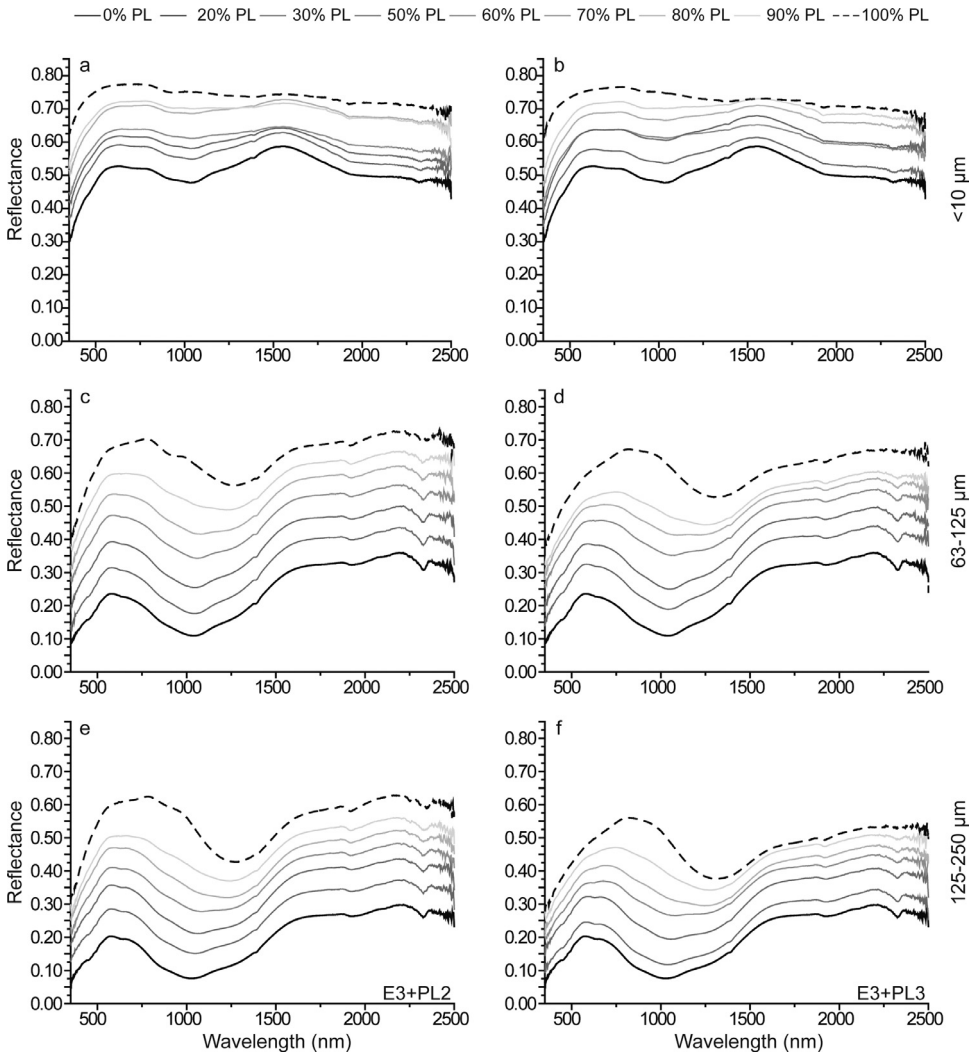

Fig. 3. Reflectance spectra of E3-PL mixtures at three different particle sizes. (a, b) E3+PL2 and E3+PL3, < 10 µm; (c, d) E3+PL2 and E3+PL3, 63–125 µm; and (e, f) E3+PL2 and E3+PL3, 125–250 µm. Generally, a fine particle size produces spectra with higher reflectance and reduced spectral contrast compared to the coarsest sizes.

To summarize, Table 3 shows that reducing the particle size (i.e., from 250 to 10 µm) of E1:

1) As mentioned above, G5 is not needed;
2) Bands are shallower, above all G1 and G3, and the Gaussians describing the different absorption bands are very similar in terms of band depth, thus reflecting the general spectral contrast;
3) G1 and G2 centers shift towards shorter wavelengths (more than 40 nm);
4) The 1850 nm absorption is fitted with only one Gaussian (G3); and
5) Band widths do not show significant changes.

Considering E3, a reduced size produces shallower bands, and a narrower G8 with respect to coarse ones; G6-G8 centers shift towards longer wavelengths, but with reduced shifts compared to E1.

G7 is the deepest one and this is not consistent with the results by Sunshine and Pieters (1998), where G8 is the deepest. However, Buz and Ehlmann (2014) demonstrated that extreme size values may affect the OL spectral parameters, which, consequently, deviate from the trend found by Sunshine and Pieters (1998). The authors showed that, at very fine sizes (<45 µm), G7 is the deepest Gaussian, also in accordance with results found by Burns (1993). However, considering E3 (Fig. 6a), G6 is slightly deeper than the results by Buz and Ehlmann (2014), but here we are dealing with even finer sizes. Furthermore, the OPX component may influence G6 depth.

The longest wavelengths of E3 are deconvolved with a Gaussian at 1963 nm, which can be tentatively assigned either to PX or to chromite (Fig. 6a; Table 3).

Table 4 reports the PL end-member spectral parameters after MGM deconvolution for the different particle sizes. MGM fits are also shown in Fig. 5g,n. In particular, reducing the size, the 1250 nm absorption can still be considered, even if, for the finest size, the band depth is close to zero. The band center shifts towards longer wavelengths both for PL2 and PL3, even if with shifts of less than 10 nm.

Table 4 shows that a coarse PL2 is deeper than the iron-richer PL3 (also refer to Serventi et al., 2015, 2016); however, the <10 µm PL3 is deeper than PL2. This can be related to the residual PX in PL2 (after magnetic separation is estimated to be less than 1%), which, at very fine sizes, becomes spectrally important, thus influencing and reducing the PL band depth. Furthermore, the residual PX produces a 900 nm absorption band that is only slightly less deep than the PL absorption band (0.015 vs. 0.026 -LnRefl, also see Fig. 3a). The 900 nm band depth in PL3, not detectable at the coarser sizes, accounts for 30% of the <10 µm PL band

Table 4
In table are reported the spectral parameters obtained by MGM deconvolution of mafic end-members, at the 63–125 μm (on the left), 125–250 μm (on the central column) and <10 μm (on the right). Center and width are expressed in nanometers, while depth as the logarithm of the reflectance. RMS represents the Root Mean Square error: the lower the RMS the better the fit. To show the goodness of the fit, for band center, the error calculated at 95% level of confidence was reported.

PL2												
	63–125 μm				125–250 μm				<10 μm			
	Center	Width	Depth	RMS	Center	Width	Depth	RMS	Center	Width	Depth	RMS
G10	1271 ± 1	505	−-0.2439		1282 ± 1	481	−0.3919		1286 ± 6	408	−0.026	
G11	1837 ± 6	443	−0.04704		1822 ± 6	441	−0.06778		1944 ± 4	250	−0.016	
G1	909 ± 2	122	−0.0395		881 ± 1	54	−0.0097		907 ± 3	129	−0.015	
				0.005				0.009				0.003
PL3												
	63–125 μm				125–250 μm				<10 μm			
	Center	Width	Depth	RMS	Center	Width	Depth	RMS	Center	Width	Depth	RMS
G10	1298 ± 2	438	−0.2356		1295 ± 2	431	−0.3598		1303 ± 5	432	−0.028	
G11	1734 ± 12	591	−0.06649		1711 ± 13	636	−0.1066		1957 ± 6	325	−0.016	
G1									941 ± 4	205	−0.01	
				0.005				0.007				0.003

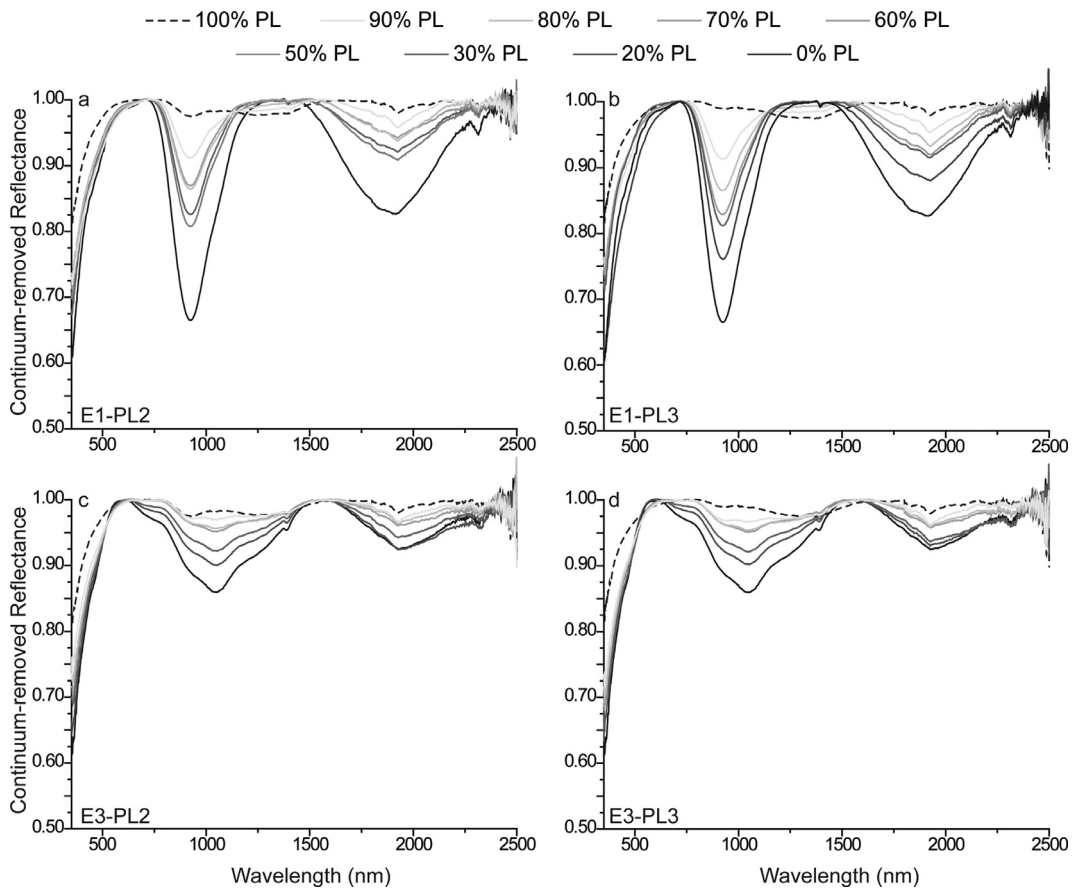

Fig. 4. End-member and mixture continuum-removed reflectance spectra. Generally, increasing the PL content in mixtures, the mafic absorptions are reduced, while the PL band behavior depends on the mafic end-member. (a, b) E1-PL2 and E1-Pl3 mixtures, respectively. PL produces an absorption bands only for very high PL content, more than 80%; (c, d) E3-PL2 and E3-Pl3, respectively. The COMP band center shifts from typical OL (1050 nm) values to PL (1250 nm) values is not detectable/noticeable.

depth (see Table 4), further evidence of the featureless behavior of fine PL.

While in the literature (e.g., Pieters, 1996; Hiroi, 2012; Serventi et al., 2015, 2016) G11 has been tentatively attributed to PL, in our work, at the <10 µm size G11 is shallower, shifts towards longer wavelengths (1940–1950 nm) and is narrower vs. the coarse sizes. Consequently, in this case, G11 probably adjusts the vibrational processes related to the OH^- alterations of the natural PL here considered.

4.3. Mixture deconvolution

Mixtures were deconvolved following the procedure described in Section 3. Fitting results, as well as RMS, are shown in Figs. 5 and 6.

PL band slightly deepens in E1 mixtures (triangles in Fig. 7a), while COMP band decreases in E3 mixtures (stars in Fig. 7a). In Fig. 7b, PL and COMP band center shifts towards longer wavelengths as the vol. FeO% in PL increases. Both PL (triangles in Fig. 7c) and COMP (stars in Fig. 7c) band widen with increasing vol. FeO% values in mixtures.

Fig. 8a and b show that increasing the vol. FeO% in PL, the Gaussians describing the mafic absorptions become shallower. Fig. 8a displays in detail the behavior described in Section 4.1, with mafic absorption bands deeper in 60%PL2-E1 and in 80%PL2-E1 than in 50%PL2-E1 and 70% Pl2-E1, respectively. However, we report the error bar for band depth, calculated in the 95% confidence interval, and it is clear that 50%PL2-E1 has a much larger error bar than 60%PL2-E1 (±0.05LnRefl vs. ±0.015LnRefl). Fig. 7b shows that the depth of Gaussians describing mafic absorptions in E3-bearing mixtures decreases more linearly than in E1-mixtures.

As stated in Section 3.4, the mafic parameters, with the exception of depth, has been kept fixed in the first iteration. Based on the residuals, we decided to leave those parameters free. Their variations have been reported in Fig. 8b,c and in Fig. 8e, for E1 and E3-bearing mixtures, respectively. Fig. 8b shows that G1 and G2 move towards longer wavelengths as PL modal abundances increases; however, G1 variations for <90% PL and G2 variations for <80% PL are less 10 nm, respectively, and, so within the instrumental spectral resolution. On the contrary, G1 and G2 shift towards longer wavelengths of 12 nm (90% PL), and of 20 nm (80% PL) and 40 nm (90% PL), respectively. These values, in particular for G2, cannot be justified by the spectral resolution, but must be related to the presence of PL, which is accommodated not only by G10 and G11. Fig. 8c reports that G3 becomes narrower with increasing PL modal abundances, while G2 varies slightly only for PL over 80%. G3 variations can be related to PL.

Regarding E3-bearing mixtures (see Fig. 8e), only G3 width varies: G3 becomes narrower as the PL content increases (with no differences between PL2 and PL3-bearing mixtures, as the values lie on the bisector line), with substantial variations for mixtures with more than 70% PL.

Fig. 9 shows a comparison for the spectral parameters after MGM deconvolution for the three different particle sizes: <10 µm (pink and violet symbols, for PL2 and PL3-bearing mixtures, respectively), 63–125 µm (light-blue and blue symbols for PL2 and PL3-bearing mixtures, respectively) and 125–250 µm (yellow and red symbols for PL2 and PL3-bearing mixtures, respectively). As al-

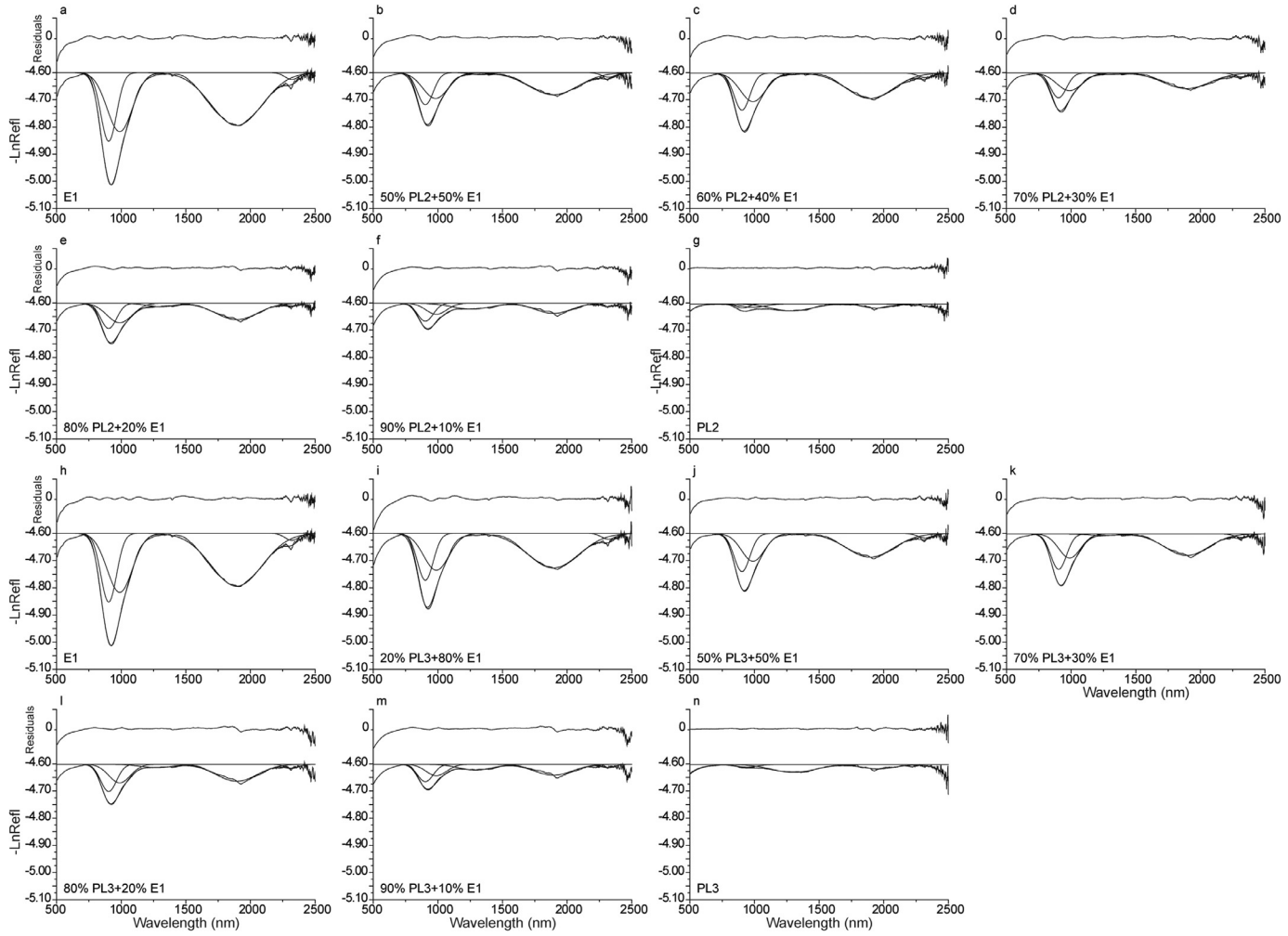

Fig. 5. MGM deconvolution and residuals of E1-bearing mixtures. RMS values are consistent with Klima et al. (2011). (a–g) E1-PL2 mixtures; (h–n) E1-PL3 mixtures. Continuum-removed reflectance is expressed as –LnRefl.

ready stated in Section 4.2, the principal difference regards band depth; Fig. 9a and d evidence that PL and COMP band are shallower than in coarser sizes, with depth close to zero. In addition, the band width in the fine particle size is strongly reduced (Fig. 9c,f), particularly in E3-bearing mixtures.

5. Discussions

In this paper we investigated the effects of a very fine particle size on the reflectance spectroscopy of PL, mafic end-members and PL-bearing mixtures.

As already stated by Adams (1968) and Pieters (1983), a fine particle size increases reflectance and decreases spectral contrast. Mustard and Hayes (1997) also evidenced that, as the size becomes finer, OL becomes brighter but shallower, and bluer in the NIR (see their Fig. 4A).

In this work, we also showed that the spectra of very fine PL become featureless, with a bluer slope than a coarse PL in the IR, and that the difference in reflectance between mixtures and end-members is reduced. Consequently, the increase in general reflectance as the PL abundance increases, documented at coarser sizes, may not be always respected. This behavior, as well as the bluer slope towards IR, similar to what happens in bulk surfaces of rocks spectra (as also postulated by Harloff and Arnold, 2001, Pompilio et al., 2007; Carli, 2009), clearly demonstrates that a very fine size could complicate the interpretation of a reflectance spectrum (e.g., slope similar for very fine size and slab of rocks), as well as the evaluation of the minerals' modal abundance.

Cheek and Pieters (2014) and Serventi et al. (2015, 2016) demonstrated that, considering PL-dominated mixtures (PL > 70/80%), Fe^{2+}-bearing PL can significantly contribute to reflectance spectra, also affecting mafic mineral absorption bands. In fact, in PX-bearing mixtures, the PL absorption band is even deeper than PX bands for very high PL content, while, in OL-bearing mixtures, the COMP band position shifts towards the typical PL center values (1250–1300 nm) for high PL content. All these effects are stronger in the 125–250 μm size than in 63–125 μm one, thus supporting that a coarse PL is spectroscopically more active than a fine one. On the contrary, this work evidences the unpredictable effects of a very fine size on reflectance spectroscopy. For example, the band depth of a very fine PL is very shallow, with Gaussian depth almost close to zero, and the COMP band center always shows the typical OL values, even for PL > 90%. This testifies that a reduced size can mask the contribution of PL on reflectance spectra, with a consequent and possible PL underestimation, which, obviously, leads to mistakes in the interpretation of reflectance spectra from a Solar System body's surface.

Furthermore, we suppose that the 1800 nm absorption detected at coarse sizes may be not found at such a fine size. In the very fine PL considered in this work, G11 is narrower and shifts towards longer wavelengths (1940–1950 nm) vs. the coarse sizes and, therefore, probably related to the OH^- alteration of the terrestrial PL.

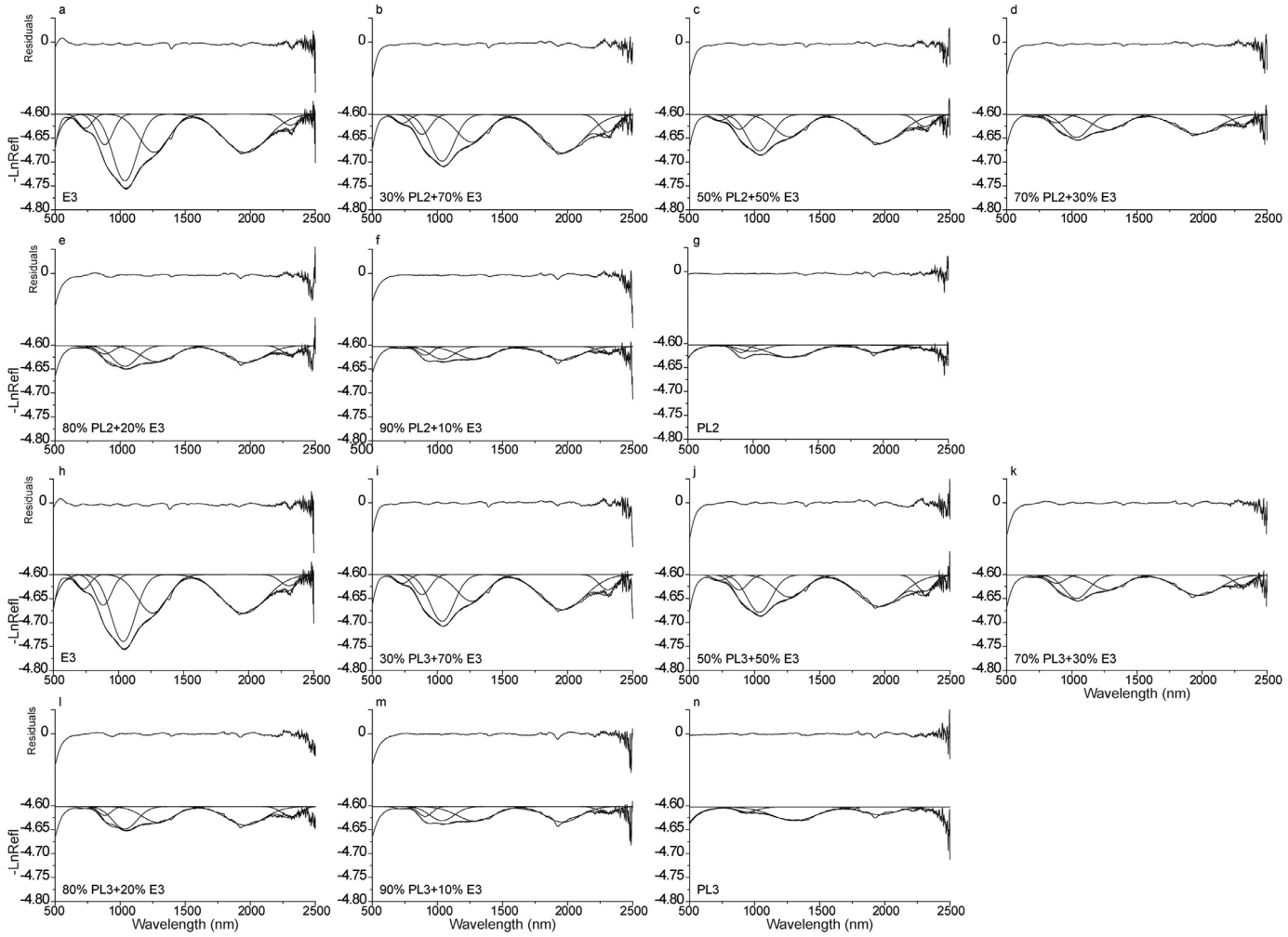

Fig. 6. MGM deconvolution and residuals of E3-bearing mixtures. RMS values are consistent with Klima et al. (2011). (a–g) E1-PL2 mixtures; (h–n) E1-PL3 mixtures. Continuum-removed reflectance is expressed as –LnRefl.

Here, we introduce an index called Band Depth Ratio (B.D.R.) calculated as follow:

$$B.D.R.(E1) = \frac{B.D.\ G10}{B.D.\ G10 + B.D.\ G1 + B.D.\ G2} \quad (1)$$

$$B.D.R.(E3) = \frac{B.D.\ G9}{B.D.\ G9 + B.D.\ G6 + B.D.\ G7} \quad (2)$$

where B.D. is the band depth of each Gaussian.

This index returns the relative intensity of PL and COMP bands with respect to all the Gaussians describing the 1000 nm absorption.

We calculated B.D.R. (E1, E3) for <10, and 63–125 and 125–250 μm (Serventi et al., 2015) sizes. Results are plotted vs. the 63–125 μm size (Fig. 10); the bisector indicates the ideal conditions in which relative depths do not change with the size. However, symbols do not lie on the bisector: 125–250 μm values (blue symbols) are in general slightly above the line, while <10 μm values (magenta symbols) are under the line. This demonstrates that, considering the 63–125 μm size as a reference, coarse PL can be slightly overestimated, and very fine PL could be easily underestimated. Moreover, as the PL abundance increases, also the difference between B.D.R. generally increases for <10 μm and for 63–125 μm. The spectral properties of mafic end-members are affected by very fine sizes, too. Regarding E1, the 900 nm absorption band is more V-shaped and more asymmetric towards the NIR vs. the coarse sizes and shifted towards shorter wavelengths, thus simulating different mineral content and/or different mineral chemistry (shorter wavelengths correspond to Mg-richer and Ca-poorer PX). The very fine E1 deconvolution does not require G5, which is, on the contrary, needed for coarser sizes (see also Pieters et al., 1993; Serventi et al., 2013).

On the other hand, the fine E3 end-member shows two main differences if compared to coarser sizes. The G6-G8 relative depths are not consistent with the trend proposed by Sunshine et al. (1998), confirming the unpredictable effects of very fine sizes; in fact, Buz and Ehlmann (2014) demonstrated that extreme sizes affect the spectral parameters of OL. Furthermore, the fine E3 longest wavelengths show absorption not detected at coarser sizes. Since E3 is characterized by 70% of OL and 30% of OPX, it seems plausible that, at very fine sizes, the presence of OPX, not detectable at coarser sizes, could become an important spectroscopic contributor.

The spectral properties seen in E1 (band center shifting), together with the behavior seen for E3 in the longest wavelengths, seem to evidence that OPX spectrally dominates at such a fine size with respect to other, mafic phases, which present a lower amount of total iron. However, E3 band can be related to residual chromite after magnetic separation.

Comparing 63–125 μm and 125–250 μm sizes, Gaussians shift less than 10 nm. The FieldSpec spectral resolution varies between

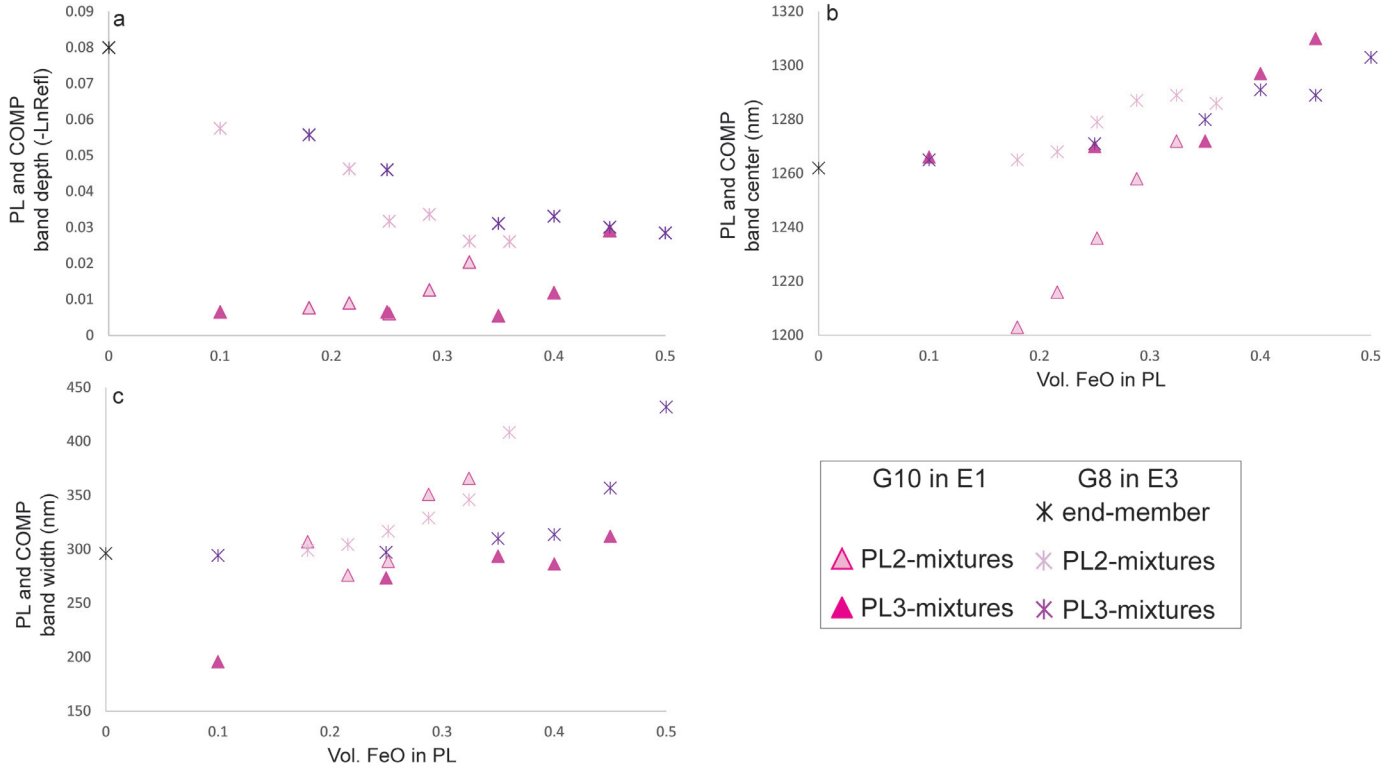

Fig. 7. The figure shows the spectral parameter variations in mixtures composed with E1/E3 and PL2,3 after MGM deconvolution. In particular, with increasing the volumetric FeO% in PL: (a) PL band deepens (triangles), while the COMP band depth decreases (stars); (b) PL band center (triangles) and COMP band center (stars) shift towards longer wavelengths (triangles); and (c) both PL (triangles) and COMP band (stars) widen.

2 and 12 nm: thus, the band center shifting falls within the instrumental resolution. On the contrary, mafic band centers for <10 μm powders are shifted of ca. 40 nm with respect to the coarser sizes; this is because we are dealing with sizes that are approximately the same size as the wavelength of light and this could lead to unexpected behaviors of the spectral parameters.

Fig. 11 reports spectra of lunar soils (from the Lunar Soil Characterization Consortium, Pieters et al., 1993, 2000) at three different fine to very fine particle sizes (20–45 μm blue spectra, 10–20 μm red spectra and <10 μm black spectra) acquired from the Apollo missions 14 and 16. In particular, samples #67,481 and #67,461 are richer in PL than samples #14,141 and #62,231. Generally, as the size decreases, reflectance increases. As expected, absorption bands are shallower and, in particular, the 1250 nm weak band becomes almost featureless in <10 μm spectra. Furthermore, Fig. 11 emphasizes the behavior of the <10 μm fractions: spectral contrast is extremely reduced if compared to the 10–20 μm size. Anyway, we have to take into account that spectra of lunar samples are affected by the presence of npFe° due to the space weathering, which implies a red slope and lower albedo than expected for PL-rich fine powders. Nevertheless, the spectra from lunar soils are in accordance with a relative increase in albedo and a strong reduction in absorptions reducing the size and an almost featureless spectrum for <10 μm size, losing information about PL absorption.

Generally, the main feature that discriminates the very fine size is the high albedo, correlated with decreasing absorption intensity. However, due to the space weathering, this feature may not be so easily recognized on lunar spectra. The low spectral contrast could be evidence of very fine size as well; however, a fine size is not the only reason to explain reduce contrasts (e.g., space weathering, shock effects).

6. Conclusion and implications for the Moon

The Moon regolith, generally <1 cm in size, comprises the lunar soil, which represents the finest fraction of the regolith and derives from mechanical disintegration of lunar rocks, both basaltic and anorthositic, and is generally between 60 and 80 μm. Very fine sizes (<10 μm) were recognized and thought to account for 5–20% of the lunar regolith; PL is the dominant phase of this fine regolith (Laul et al., 1978, 1979, 1980).

In this work, we demonstrated that a very small size implies higher albedo and a decrease in spectral contrast, particularly for the PL spectra that become almost featureless. On the other hand, we showed that the iron-richest mineral in the considered mixtures, OPX, seems to spectrally dominate other mafic and cogenetic minerals, CPX and OL, at the very fine size (e.g., the 900 nm band shifts towards shorter wavelengths in E1 and the 2000 nm reflectance decreases in E3).

This has important implications for the lunar regolith, where PL is abundant. For example, the presence of PL spectra with a well-defined and deep 1250 nm absorption gives indications not only on the crystallinity of the mineral but also on the particulate size that cannot be too fine in the areas were PL absorption is detected. On the other hand, featureless PL spectra can lead to an erroneous interpretation of the PL abundance and/or chemistry, which can be underestimated. These results evidence that more detailed investigations on such fine sizes should be pursued to better understand how to retrieve composition by modeling remote sensing data.

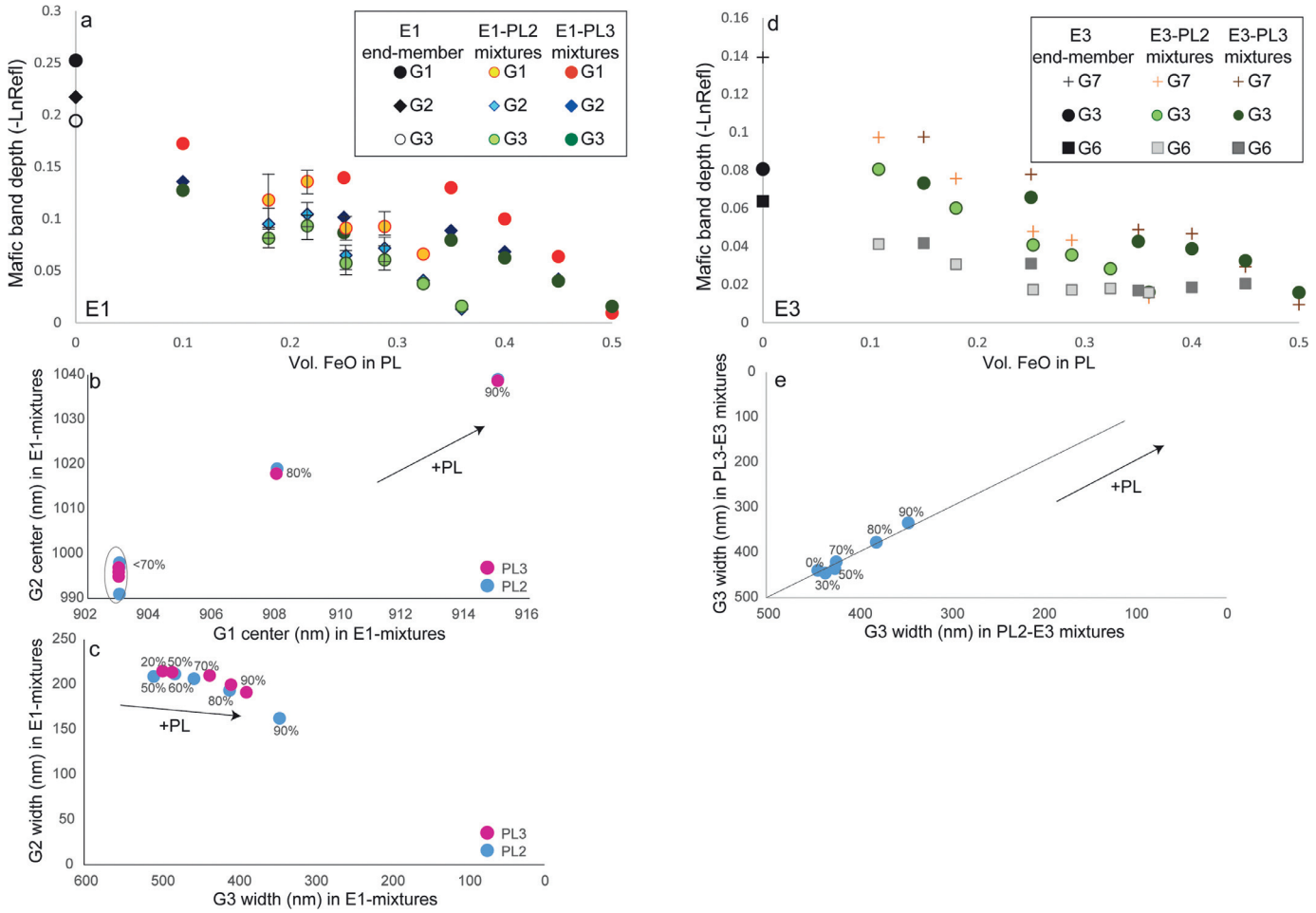

Fig. 8. The figure shows the spectral parameter variations in mixtures composed with E1/E3 and PL2,3 after MGM deconvolution. In particular, with increasing the volumetric FeO% in PL: (a, d) the mafic band depth decreases both in E1 and in E3-bearing mixtures. Fig. 8a also shows the vertical error bars for the 50–80% PL2-E1 mixtures; (b) G1 and G2 move towards longer wavelengths with increasing PL modal abundances. G1 variations and G2 variations for <80% PL are less than 10 nm and, so, explainable by the instrument spectral resolution; G2 shifts for 80% and 90% PL can be related to the presence of PL; (c) G3 become narrower with increasing PL modal abundances, while G2 varies only slightly; only G2 variations for more than 70% PL2 can be related to PL, while other variations are, again, explainable with the instrument spectral resolution; and (e) G3 becomes narrower with increasing the PL content (with no differences between PL2 and PL3-bearing mixtures, as the values lay on the bisector line), but variations are substantial only for more than 80% PL.

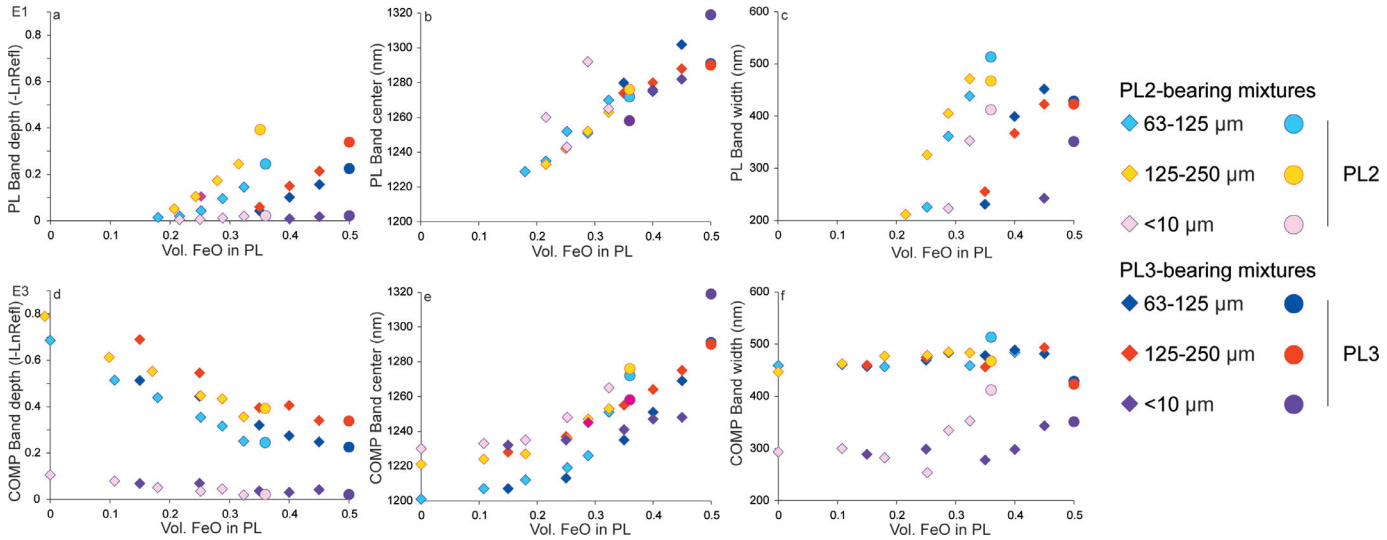

Fig. 9. The figure shows a comparison for the spectral parameters after MGM deconvolution for the three different particle sizes: <10 µm (violet symbols), 63–125 µm (pink symbols) and 125–250 µm (fuchsia symbols). (a, d) PL (in E1-bearing mixtures) and COMP (in E3-bearing mixtures) band depths are very reduced compared to the coarse sizes and close to zero; (b, e) the PL band center does not show great variations in E1-bearing mixtures, while in E3-PL2 mixtures the COMP band center is shifted towards longer wavelengths. On the contrary, is shifted towards shorter wavelength in E3-PL3 mixtures; and (c, f) the band width in the fine particle size is strongly reduced, particularly in the E3-bearing mixtures. (For interpretation of the references to colour in this figure legend, the reader is referred to the web version of this article.)

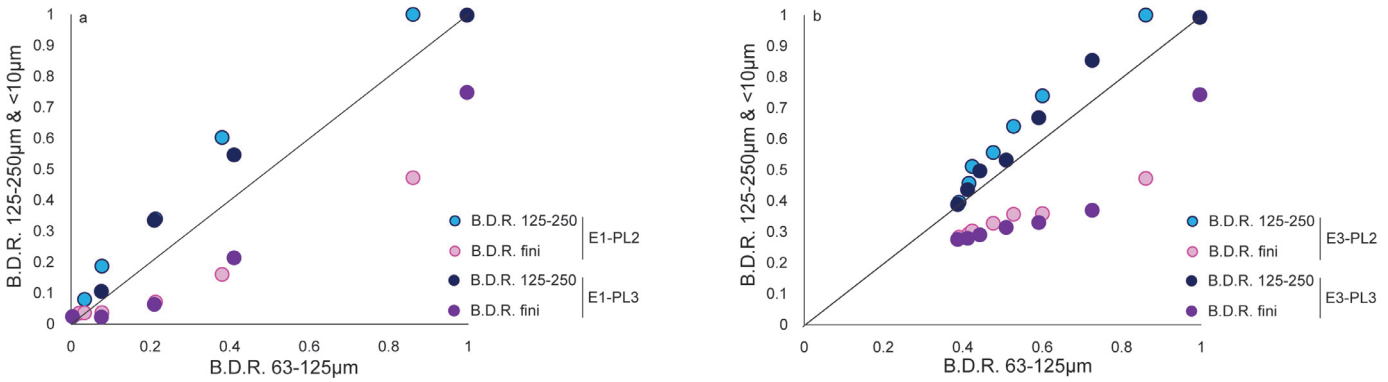

Fig. 10. Band Depth Ratio (B.D.R.) for the 125–250 µm and <10 µm sizes vs. the 63–125 µm size. (a) E1-bearing mixtures; (b) E3-bearing mixtures. The bisector indicates the ideal conditions that the relative depths do not change with the size; however, 125–250 µm values (blue symbols) stay above the line, while <10 µm values (magenta symbols) are under the line. (For interpretation of the references to colour in this figure legend, the reader is referred to the web version of this article.)

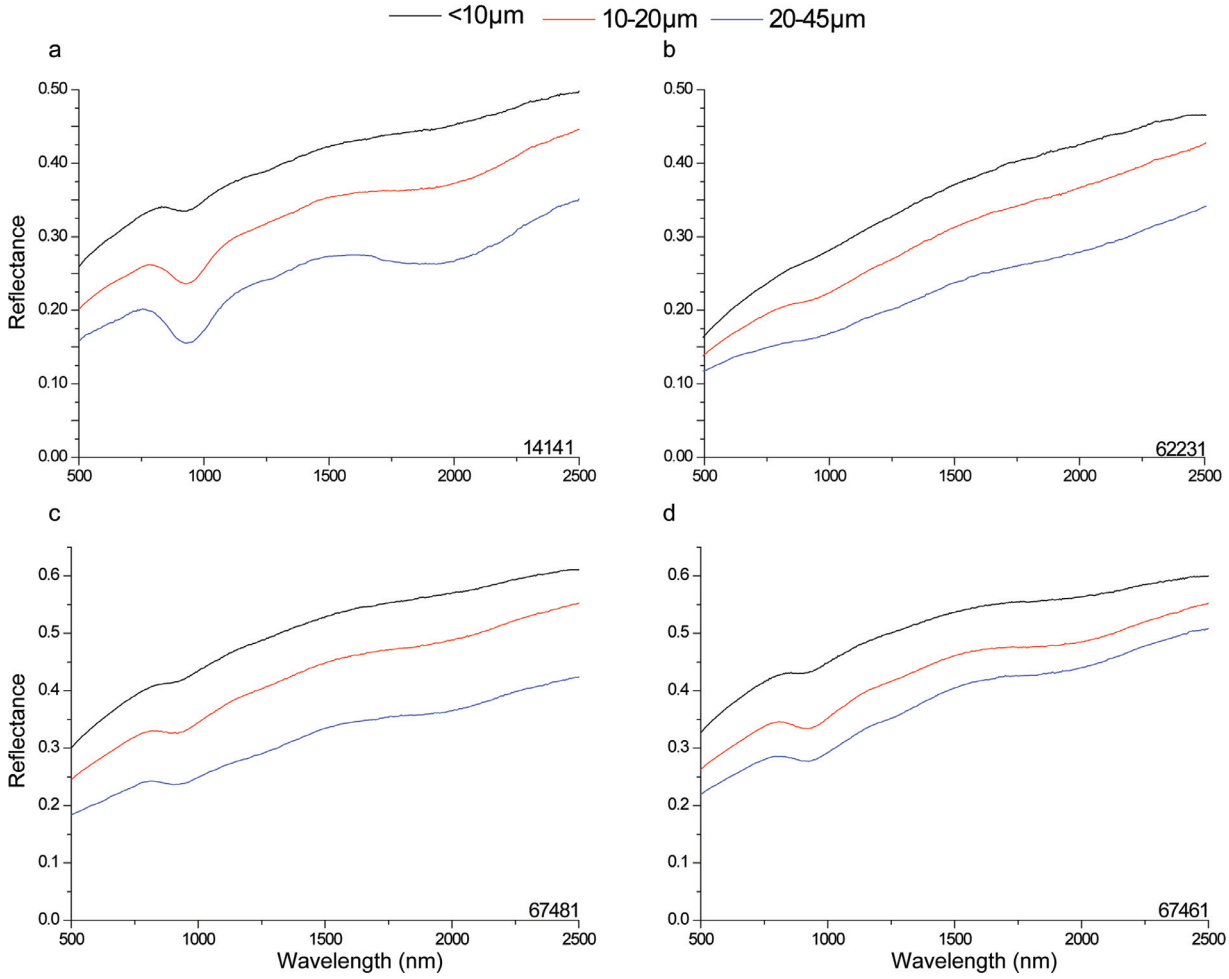

Fig. 11. Spectra of lunar soils (from the Lunar Soil Characterization Consortium, from Pieters et al. (1993, 2000) at three different, very fine particle sizes (20–45 µm blue spectra, 10–20 µm red spectra and <10 µm black spectra). Samples #67,481 and #67,461 are more enriched in PL than samples #14,141 and #62,231.Generally, reducing the size the reflectance increases, absorption bands are shallower and, in particular, the 1250 nm band becomes almost featureless in <10 µm spectra. (For interpretation of the references to colour in this figure legend, the reader is referred to the web version of this article.)

Acknowledgment

Spectroscopic measurements were carried out at Inaf-IAPS-Istituto Nazionale di Astrofisica, Roma. EMPA analyses and powder micronization have been performed at Dipartimento di Geoscienze, Padua, Italy. The authors are grateful to prof. Maria Sgavetti for her thoughtful review that greatly improved the quality of the manuscript. The authors are also grateful to two anonymous reviewers for their stimulating comments and suggestions.

References

Adams, J.B., 1968. Lunar and Martian surfaces: petrologic significance of absorption bands in the near-infrared. Science 159, 1453–1455.

Adams, J.B., Goulland, L.H., 1978. Plagioclase feldspar: visible and near infrared diffuse reflectance spectra as applied to remote sensing. Proc. Lunar Sci. Conf. 3, 2901–2909.
Burns, R.G., 1993. Mineralogical Applications of Crystal Field Theory. Cambridge University Press, Cambridge, p. 551.
Buz, J., Ehlmann, L., 2014. Effects of grain size on the reflectance spectroscopy of olivine in the VIS-NIR and the derivation of olivine composition using modified Gaussian modeling. Lunar. Planet. Sci. 45. Abstract 2810.
Carli, C., 2009. Spectral analyses in the VNIR of igneous rocks: surface composition characterization of terrestrial planets. Plinius 35, 83–90.
Carli, C., Ciarniello, M., Capaccioni, F., Serventi, G., Sgavetti, M., 2014. Spectral variability of plagioclase-mafic mixtures (2): investigation of the optical constant and retrieved mineral abundance dependence on particle size distribution. Icarus 235, 207–219.
Cheek, L.C., Pieters, C.M., Parman, S.W., Dyar, M.D., Speicher, E.A., Cooper, R.F., 2011. Spectral characteristics of PL with variable iron content: application to the remote sensing of the lunar crust. Lunar. Planet. Sci. 42. Abstract 1617.
Cheek, L.C., Pieters, C.M., 2012a. Variations in anorthosite purity at Tsiolkovsky crater on the Moon. Lunar. Planet. Sci. 43. Abstract 2624.
Cheek, L.C., Donaldson Hanna, K.L., Pieters, C.M., Head, J.W., Whitten, J.L., 2012b. The distribution and mineralogy of anorthosite in the Orientale Basin: new perspective from M^3 data. Second Conference on the Lunar Highland Crust. Abstract 9022.
Cheek, L.C., Pieters, C.M., 2014. Reflectance spectroscopy of plagioclase-dominated mineral mixtures: implication for characterizing lunar anorthosites remotely. Am. Min. 99, 1871–1892.
Clenet, H., et al., 2011. A new systematic approach using the Modified Gaussian Model: insight for the characterization of chemical composition of olivines, pyroxenes and olivine-pyroxene mixtures. Icarus 213, 404–422.
Cloutis, E.A., Sunshine, J.M., Morris, R.V., 2004. Spectral reflectance-compositional properties of spinels and chromites: implications for planetary remote sensing and geothermometry. Meteorit. Planet. Sci. 39, 545–565.
Cooper, C.D., Mustard, J.F., 1999. Effects of very fine particle size on reflectance spectra of smectite and palagonitic soil. Icarus 142, 557–570.
Craig, M.A., Cloutis, E.A., Bailey, D.T., 2007. The effects of grain size, <45–1000 μm, on the reflectance spectrum of planetary analogs from 0.35–2.5 μm. Lunar. Planet. Sci. 38. Abstract 1356.
Crown, D.A., Pieters, C.M., 1987. Spectral properties of PL and pyroxene mixtures and the interpretation of lunar soil spectra. Icarus 72, 492–506.
Devine, J.M., McKay, D.S., Papike, J.J., 1982. Lunar regolith: petrology of the <10 μm fraction. In: Proc. Lunar Planet Sci. Conf. 13th, pp. A260–A268.
Harloff, J., Arnold, G., 2001. Near-infrared reflectance spectroscopy for bulk analog materials for planetary crust. Planet. Space Sci. 49, 191–211.
Hiroi, T., et al., 2012. Diversity in the visible-NIR absorption band characteristics of lunar and asteroidal plagioclase. Lunar. Planet. Sci. 43. Abstract 1168.
Klima, R.L., Pieters, C.M., Dyar, D.M., 2007. Spectroscopy of synthetic Mg-Fe pyroxenes I: Spin-allowed and spin-forbidden crystal field bands in the visible and near-infrared. Meteorit. Planet. Sci. 42, 235–253.
Klima, R.L., Dyar, D.M., Pieters, C.M., 2011. Near-infrared spectra of clinoyroxenes: effect of calcium content and crystal structure. Meteorit. Planet. Sci. 46, 279–295.
Kramer, G.Y., Kring, D.A., Mahm, A.L., Pieters, C.M., 2013. Spectral and photogeologic mapping of Schrödinger Basin and implications for post-South Pole-Aitken impact deep subsurface stratigraphy. Icarus 223, 131–148.
Laul, J.C., Vaniman, D.T., Papike, J.J., Simon, S.B., 1978. Chemistry and petrology of size fractions of Apollo 17 deep drill core 70009-70006. In: Proc. Lunar Planet Sci. Conf. 9th, pp. 2065–2097.
Laul, J.C., Lepel, E.A., Vaniman, D.T., Papike, J.J., 1979. The Apollo 17 drill core: chemical systematics of grain size fractions. In: Proc. Lunar Planet Sci. Conf. 10th, pp. 1269–1298.
Laul, J.C., Papike, J.J., 1980. The lunar regolith: comparative chemistry of the Apollo sites. In: Proc. Lunar Planet Sci. Conf. 11th, pp. 1307–1340.
McKay, D.S., Heiken, G., Basu, A., Blanford, G., Simon, S., Reedy, R., French, B.M., Papike, J., 1991. The lunar regolith. In: Heiken, G.H., Vaniman, D.T., French, B.M. (Eds.), Lunar Sourcebook: a User's Guide to the Moon. Cambridge University Press, Cambridge, pp. 285–356.
Mustard, J.F., Hays, J.E., 1997. Effects of hyperfine particles on reflectance spectra from 0.3 to 25 μm. Icarus 125, 145–163.
Nash, D.B., Conel, J.E., 1974. Spectral reflectance systematics for mixtures of powdered hypersthene, labradorite, and ilmenite. J. Geophys. Res. 79, 1615–1621.
Ohtake, M., et al., 2009. The global distribution of pure anorthosite on the Moon. Nature 461. doi:10.1038/nature08317.
Papike, J.J., Taylor, L.A., Simon, S., 1991. Lunar minerals. In: Heiken, G., Vaniman, D., French, B. (Eds.), The Lunar Sourcebook. Cambridge Univ. Press, New York, pp. 121–181.
Pieters, C.M., Fischer, E.M., Rode, O., Basu, A., 1993. Optical effects of space weathering: the role of the finest fraction. J. Geophys. Res. 98, 20817–20824.
Pieters, C.M., 1983. Strength of mineral absorption features in the transmitted component of near-infrared reflected light: First results from RELAB. J. Geophys. Res. 88, 9534–9544.
Pieters, C.M., 1986. Composition of the lunar highland crust from near-infrared spectroscopy. Rev. Geophys. 24, 557–578.
Pieters, C.M., 1996. Plagioclase and maskelynite diagnostic features. Lunar. Planet. Sci. 27, Abstract 1031.
Pieters, C.M., et al., 2000. Space weathering on airless bodies: resolving a mystery with lunar samples. Meteor. Planet. Sci. 35.
Pompilio, L., Sgavetti, M., Pedrazzi, G., 2007. Visible and near-infrared reflectance spectroscopy of pyroxene-bearing rocks: new constraints for understanding planetary surface compositions. JGR 112, E01004. doi:10.1029/2006JE002737.
Serventi, G., Carli, C., Sgavetti, M., Ciarniello, M., Capaccioni, F., Pedrazzi, G., 2013. Spectral variability of plagioclase-mafic mixtures (1): effects of chemistry and modal abundance in reflectance spectra of rocks and mineral mixtures. Icarus 226, 282–298. doi:10.1016/j.icarus.2013.05.041.
Serventi, G., Carli, C., Sgavetti, M., 2015. Spectral variability of plagioclase-mafic mixtures (3): quantitatively analysis appling the MGM algorithm. Icarus 254, 34–55. doi:10.1016/j.icarus.2015.03.024.
Serventi, G., Carli, C., Sgavetti, M., 2016. Deconvolution of mixtures with high plagioclase content for the remote interpretation of lunar plagioclase-rich regions. Icarus 272, 1–15. doi:10.1016/j.icarus.2016.01.020.
Spudis, P.D., Hawke, B.R., Lucey, P.G., 1984. Composition of orientale basin deposits and implications for the lunar basin-forming process. J. Geophys. Res. 89, 197–210.
Sunshine, J.M., Pieters, C.M., Pratt, S.F., 1990. Deconvolution of mineral absorption bands: an improved approach. J. Geophys. Res. 95, 6955–6966.
Sunshine, J.M., Pieters, C.M., 1993. Estimating modal abundances from the spectra of natural and laboratory pyroxene mixtures using the Modified Gaussian Model. J. Geophys. Res. 98, 9075–9087.
Sunshine, J.M., Pieters, C.M., 1998. Determining the composition of olivine from reflectance spectroscopy. J. Geophys. Res. 103, 13675–13688.
Tompkins, S., Pieters, C.M., 1999. Mineralogy of the lunar crust: results from Clementine. Meteorit. Planet. Sci. 34, 25–41.